DISCLAIMER

This report was prepared as an account of work sponsored by an agency of the United States Government. Neither the United States Government nor any agency thereof, nor any of their employees, makes any warranty, express or implied, or assumes any legal liability or responsibility for the accuracy, completeness, or usefulness of any information, apparatus, product, or process disclosed, or represents that its use would not infringe privately owned rights. Reference herein to any specific commercial product, process, or service by trade name, trademark, manufacturer, or otherwise does not necessarily constitute or imply its endorsement, recommendation, or favoring by the United States Government or any agency thereof. The views and opinions of authors expressed herein do not necessarily state or reflect those of the United States Government or any agency thereof. Reference herein to any social initiative (including but not limited to Diversity, Equity, and Inclusion (DEI); Community Benefits Plans (CBP); Justice 40; etc.) is made by the Author independent of any current requirement by the United States Government and does not constitute or imply endorsement, recommendation, or support by the United States Government or any agency thereof.

SAND2025-14908

SANDIA REPORT

SAND20XX-XXXX
Printed August 2025

Sandia National Laboratories

Assessing Dynamic Time Warping Techniques for Discriminating Seismic Sources at Local and Regional Distances

G. Didem Beskardes, Rigobert Tibi and Christopher J. Young

Prepared by
Sandia National Laboratories
Albuquerque, New Mexico
87185 and Livermore,
California 94550

Issued by Sandia National Laboratories, operated for the United States Department of Energy by National Technology & Engineering Solutions of Sandia, LLC.

Available to DOE and DOE contractors from
U.S. Department of Energy
Office of Scientific and Technical Information
P.O. Box 62
Oak Ridge, TN 37831

Telephone: (865) 576-8401
Facsimile: (865) 576-5728
E-Mail: reports@osti.gov
Online ordering: http://www.osti.gov/scitech

Available to the public from
U.S. Department of Commerce
National Technical Information Service
5301 Shawnee Rd
Alexandria, VA 22312

Telephone: (800) 553-6847
Facsimile: (703) 605-6900
E-Mail: orders@ntis.gov
Online order: https://classic.ntis.gov/help/order-methods/

ABSTRACT

Effective monitoring of seismic explosions and hazard assessment relies heavily on the accurate discrimination of underground seismic sources. This study investigates the application of novel nonlinear alignment techniques, specifically Dynamic Time Warping (DTW), for event-type discrimination at regional and local distances. Building on prior research that used DTW and Elastic Shape Analysis (ESA) in discrimination at regional distances, we evaluate the performance of recently developed variants of DTW, including a method that employs Pearson cross-correlation as a measure of warping distance and a time distortion coefficient that quantifies the type and degree of time distortion between signals.

By analyzing observational datasets that include different source types, we assess the performance of these approaches for realistic monitoring scenarios. Specifically, we consider a dataset recorded at regional distances in the Korean Peninsula and a local-distance subset from the Unconstrained Utah Event Bulletin catalog to evaluate DTW-based discrimination across multiple distance scales. Additionally, we introduce the maximum cross-correlations of warped waveforms as a similarity metric for event classification. Through hierarchical cluster analysis and dendrogram interpretation, we present our findings, highlighting the strengths and limitations of these techniques in seismic event classification.

ACKNOWLEDGEMENTS

This Ground-based Nuclear Detonation Detection (GNDD) research was funded by the National Nuclear Security Administration, Defense Nuclear Nonproliferation Research and Development (NNSA DNN R&D). Sandia National Laboratories is a multimission laboratory managed and operated by National Technology and Engineering Solutions of Sandia, LLC, a wholly owned subsidiary of Honeywell International, Inc., for the U.S. Department of Energy's National Nuclear Security Administration under contract DE-NA-0003525. The views expressed in the article do not necessarily represent the views of the U.S. Department of Energy or the United States Government. We thank Erica Emry for a thoughtful technical review of this report.

CONTENTS

Abstract....3
Acknowledgements....4
Acronyms and Terms....8
1. Introduction....9
   1.1. Dynamic Time Warping (DTW)....9
2. Evaluating DTW-based discrimination at regional scales....11
   2.1. DTW with Pearson cross-correlation and time distortion coefficient....11
   2.2. Clustering the cross-correlation of warped signals....19
3. Evaluating DTW-based discrimination at local scales....21
4. Conclusions....28
References....29
Distribution....31

LIST OF FIGURES

Figure 2-1. a) Vertical-component waveforms recorded at station MDJ filtered between 0.5 and 3 Hz. EQ1 and EQ2 are the earthquake pairs, $\boldsymbol{mb}$ 2.5 and 3.6, respectively. NK1 is the 2006 declared nuclear explosion test and CO is the collapse event that followed the 2017 declared nuclear explosion test. Waveforms aligned according to EQ1 are plotted by using b) DTW and c) ESA. The warping paths between each signal pair for d) DTW and e) ESA alignment, respectively. The DTW distance and the phase ($\boldsymbol{Dx}$) and amplitude ($\boldsymbol{Dy}$) of ESA are indicated in the lower right corners. f) The CC before (squares) and after DTW (diamond) and ESA (cross) alignment. 12
Figure 2-2. The warping paths and aligned waveforms, the CC (before (squares) and after alignments) between each signal pair by using DTW-pcc with a correlation time windows of a) 1 s, b) 2 s and c) 4 s. DTW distances are listed as inset....13
Figure 2-3. DTW and TDC distances for each event pair in Figure 2-1 obtained from a) traditional DTW, and DTW-pcc using correlation time windows of b) 1 s and c) 2 s....14
Figure 2-4. Vertical-component waveforms recorded at station MDJ filtered between 0.8 and 5 Hz, including earthquakes (0 — 12), explosions (13 — 18) and collapse (19). The explosions are the declared 2006 (NK1), 2009 (NK2), 2013 (NK3), 2016 (NK4, NK5), and 2017 (NK6) nuclear tests in the Korean Peninsula....15
Figure 2-5. a) Phase ($\boldsymbol{Dx}$) and b) amplitude ($\boldsymbol{Dy}$) distance of ESA and c) DTW distance between every earthquake and explosion signal pair. Their corresponding dendrograms from hierarchical clustering analysis are shown in d) and e), respectively. f) Warping distances of each signal pair obtained using DTW-pcc ($\boldsymbol{2L = 2}$ s) and g) its dendrogram. 16
Figure 2-6. Vertical-component waveforms recorded at station MDJ (in Figure 2-4) filtered within a lower frequency band of 0.5 and 3 Hz. 17
Figure 2-7. a) Phase ($\boldsymbol{Dx}$) and b) amplitude ($\boldsymbol{Dy}$) distance of ESA and c) DTW distance between every earthquake and explosion signal pair filtered with a lower frequency band (Figure 2-6). Their corresponding dendrograms from hierarchical clustering analysis are shown in d) and e), respectively. f) Warping distances of each signal pair obtained using DTW-pcc ($\boldsymbol{2L = 2}$ s) and g) its dendrogram....18

Figure 2-8. TDC distances between each signal pair in Figure 2-4 obtained using a) traditional DTW and b) DTW-pcc ($2L = 2$ s). 19
Figure 2-9. a) CC before alignment, b) after ESA and c) DTW alignments for each signal pair in Figure 2-4, along with their corresponding dendrograms from hierarchical clustering analysis. ..20
Figure 3-1. UUEB catalog events. The map (right) provides a closer view of the events. Clusters highlighted by dashed squares are included in the analysis. Black triangles indicate some of the nearby stations. 21
Figure 3-2. a) Vertical-component waveforms recorded at station SNUT filtered between 2 and 10 Hz. b) Phase (Dx) and c) amplitude (Dy) distance of ESA and d) DTW distance between every earthquake and explosion-like event pairs. 22
Figure 3-3. a) CC before alignment, b) after ESA and c) DTW alignments for each signal pair in Figure 3-2, along with their corresponding dendrograms from hierarchical clustering analysis. The black dots indicate the events that were misclassified in the dendrogram. 23
Figure 3-4. Vertical-component waveforms recorded at station EPU filtered between 2 and 10 Hz. b) Phase (Dx) and c) amplitude (Dy) distance of ESA and d) DTW distance between every earthquake and explosion-like event pairs. 24
Figure 3-5. a) CC before alignment, b) after ESA and c) DTW alignments for each signal pair in Figure 3-4, along with their corresponding dendrograms from hierarchical clustering analysis. The black dots indicate the events that were misclassified in the dendrogram (not shown for DTW). 25
Figure 3-6. Following the exclusion of waveforms with noise spikes, a) CC before alignment, b) after ESA and c) DTW alignments for each signal pair in Figure 3-4, along with their corresponding dendrograms from hierarchical clustering analysis. The black dots indicate the events that were misclassified in the dendrogram (not shown for DTW). 26
Figure 3-7. a) A pair of earthquake waveforms recorded at station GZU, displayed without any warping, alongside the aligned pairs obtained using DTW and ESA. b) The warping paths of DTW and ESA between the signal pair and the CC before (squares) and after DTW (diamond) and ESA (cross) alignment. 27

This page left blank

ACRONYMS AND TERMS

Acronym/Term	Definition
CC	Normalized, maximum cross-correlation coefficient
DTW	Dynamic Time Warping
ESA	Elastic Shape Analysis
UUEB	Unconstrained Utah Event Bulletin

1. INTRODUCTION

Accurately discriminating between different underground seismic sources at variable observational distances (local, regional, and teleseismic) is crucial for both seismic explosion monitoring and hazard assessment. Traditional discriminant approaches are based on the theoretical differences in wave excitation between earthquake and explosion-like sources. These methods include moment tensor inversion [1] [2], amplitude ratios of body waves to surface waves [3] [4] [5], and their combinations with other physics-based metrics [6] [7]. In addition, machine learning techniques have also been applied to local and near-regional datasets [8] [9] [10] [11] [12]. However, the success of these methods is influenced by various factors. In amplitude-based discrimination approaches, challenges include isolating the source terms from propagation path effects and site effects [10], as well as the absence of certain phases in some regions and difficulties in phase separation particularly at local distances [9] [13]. For machine learning methods, a significant limitation is the lack of existing labeled datasets for specific regions.

As an alternative, Dynamic Time Warping (DTW) and Elastic Shape Analysis (ESA), both recognized as nonlinear alignment algorithms, have been considered for informing event discrimination through their amplitude and phase warping distances. A previous study demonstrated the potential of these algorithms for discrimination by applying them to recorded regional-distance waveforms from different types of seismic sources in the Korean Peninsula [14]. Building on this foundation for regional source-type discrimination, we evaluate the performance of these techniques, along with their recently-developed variants, in the context of event-type discrimination at both regional and local scales in this report.

Research on DTW is rapidly advancing (e.g., fastDTW [15], subsequence DTW [16], shapeDTW [17]). In our work, we consider two advanced approaches that were not investigated in the previous study: a DTW method that utilizes Pearson cross-correlation as a warping distance [18] and a time distortion coefficient that serves as a metric for the type and degree of time distortion between time series [19]. First, we evaluate the performance of both approaches using the observational dataset of earthquake, explosion, and collapse events from the Korean Peninsula that was used in the previous study. Additionally, we propose using the maximum cross-correlations (CCs) of the warped waveforms as similarity metric in event classification, instead of DTW and ESA distances. Next, we apply our methods to a subset of waveform data from the Unconstrained Utah Event Bulletin (UUEB) [20], which consists of explosion-like and earthquake sources, to assess the performance of DTW-based discrimination at local distances. We present the performance of event discrimination by applying hierarchical cluster analysis and interpret the findings through dendrograms.

1.1. Dynamic Time Warping (DTW)

The DTW is used to estimate time shifts necessary for an optimal alignment of the time series with different lengths [21]. Given two time series $f_1(t)$ and $f_2(t)$ of length m and n respectively, the first step of DTW is to construct the cumulative distance matrix $\boldsymbol{D}$ that contains distances between two time series at different time delays which are calculated by the following recurrence formula:

$$\boldsymbol{D}(i,j) = \begin{cases} d(i,j) & i = 1, j = 1 \\ d(i,j) + D(i,j-1) & i = 1, j > 1 \\ d(i,j) + D(i-1,j) & i > 1, j = 1 \\ d(i,j) + min\begin{cases} D(i-1,j-1) \\ D(i-1,j) \\ D(i,j-1) \end{cases} & i > 1, j > 1 \end{cases} \quad (1)$$

where $1 \le i \le m$ and $1 \le j \le n$. The local distance $d(i,j)$ is traditionally calculated as the squared Euclidean distance $(f_1^i - f_2^j)^2$. After computing the cumulative distance matrix, the DTW warping path with the smallest accumulated distance can be easily obtained [22].

DTW warping distances are commonly used as a similarity metric. For seismic data recorded by a given deployed sensor, smaller DTW distances are expected while warping the signals generated by the same seismic source type compared to those from different source types. Therefore, those DTW distances can be used as a proxy for source discrimination, assuming that the seismic sources are closely located and the differences in the signal phase and amplitude are mainly due to the source type [14]. Traditional DTW imposes challenges in capturing amplitude changes (e.g., body and surface waves) while performing more efficiently for phase variability [22]. On the other hand, ESA is more robust for both phase and amplitude variability within a time series by separating the phase and amplitude distances [23]. Cluster analyses from the previous study indicate that DTW and ESA demonstrated modest classification accuracy for observed seismic signals from earthquakes and explosions recorded at regional distances [14], motivating our additional research described in this report.

2. EVALUATING DTW-BASED DISCRIMINATION AT REGIONAL SCALES

2.1. DTW with Pearson cross-correlation and time distortion coefficient

We implemented two recently developed DTW approaches and evaluate their efficiency in source discrimination. The first approach utilizes the Pearson correlation coefficient (CC) as the warping distance metric. This approach has been successfully applied to seismic waveforms recorded at regional distances, enhancing the imaging resolution of the back-projection of seismic events and improving the accuracy of their locations [18]. The conventional use of Euclidean distance in DTW may not adequately capture variations in both amplitude and phase of seismic signals, particularly given the differing epicentral distances and seismic source radiation patterns. To better align signals from different stations, the authors propose employing the Pearson CC as the local distance $d(i,j)$ in Eq.1 as

$$Pearson\ CC = 1 - \frac{\sum_{i=-L}^{L}[x_1(t)-\overline{x_1}][x_2(t+s)-\overline{x_2}]}{\sqrt{\sum_{i=-L}^{L}[x_1(t)-\overline{x_1}]^2 \sum_{i=-L}^{L}[x_2(t)-\overline{x_2}]^2}}. \quad (2)$$

Here, L is half the size of a time window used for calculating the Pearson CC at different time delays in Eq.1 and should be smaller than the signal period. We will refer this time window as the correlation time window.

Instead of utilizing DTW with Pearson CC distance for more coherent stacking of signals from different stations during earthquake back-projection [18], we assess its performance in clustering different types of seismic sources using signals from a single station. We consider a previously analyzed real seismic dataset from a small region in the Korean Peninsula that includes explosions, naturally occurring earthquakes, and collapse events, with all events located within a 10 km epicentral distance of one another [24]. This is the same dataset that was used in the previous DTW/ESA source discrimination study [14], and to ensure a fair performance comparison with that previous study, we use the same subset of waveforms for our tests, which consists of signals from closely spaced events recorded at a single station.

Four vertical-component broadband waveforms recorded at station MDJ (Network IC) were selected: two from naturally occurring earthquakes (EQ1 and EQ2), one from the 2006 declared nuclear test (NK1), and one from a collapse event following the largest declared nuclear test in 2017 (Figure 2-1a). The waveforms were obtained from the Incorporated Research Institutions for Seismology (IRIS) and filtered between 0.5 and 3 Hz. The DTW and ESA methods optimally align the signal pairs with varying rates of compression and stretch (Figure 2-1b and c). As demonstrated in [14], both DTW and ESA yield the smallest distances for the earthquake pair (Figure 2-1d and e), while DTW significantly increases the similarity (CC) between each signal pair, regardless of the source types (Figure 2-1f).

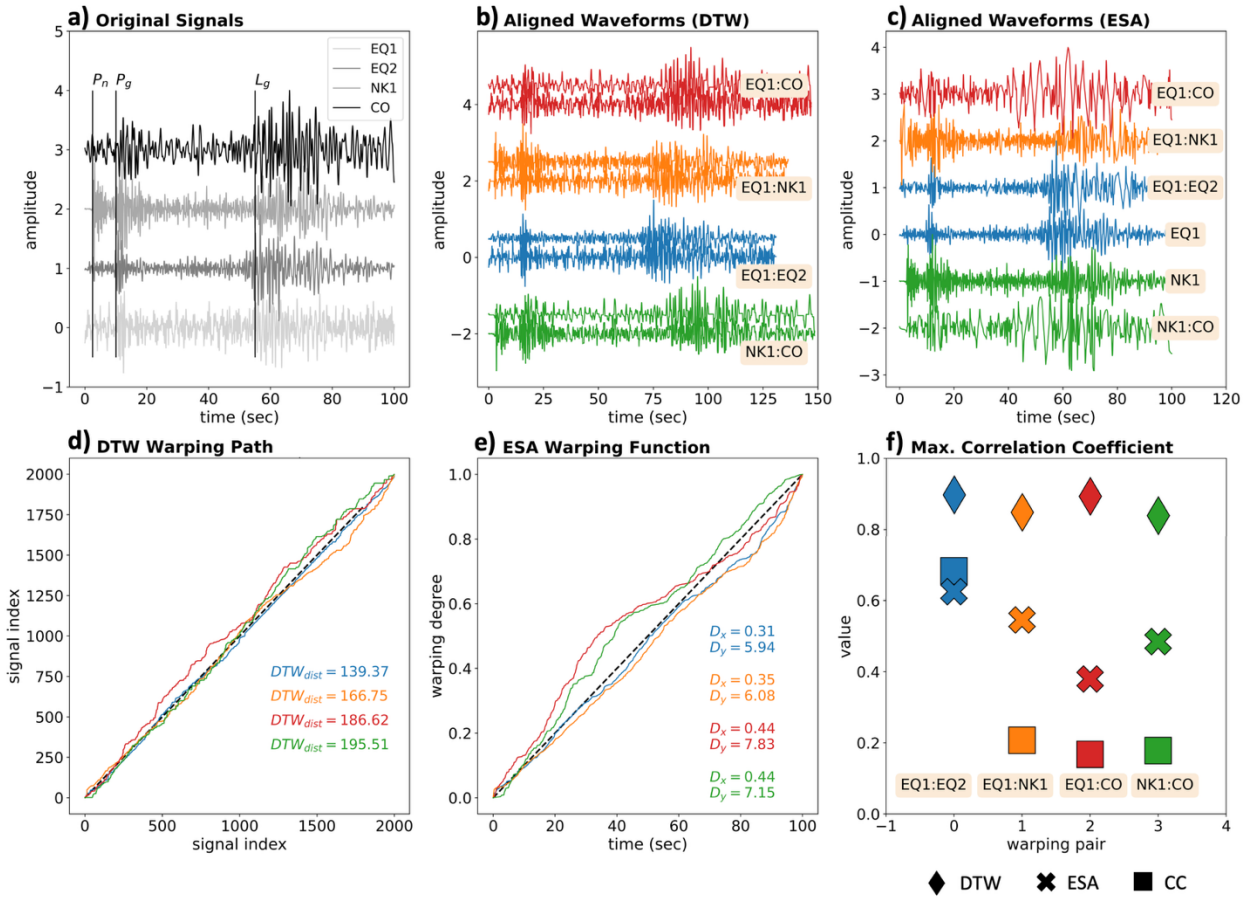

Figure 2-1. a) Vertical-component waveforms recorded at station MDJ filtered between 0.5 and 3 Hz. EQ1 and EQ2 are the earthquake pairs, m_b 2.5 and 3.6, respectively. NK1 is the 2006 declared nuclear explosion test and CO is the collapse event that followed the 2017 declared nuclear explosion test. Waveforms aligned according to EQ1 are plotted by using b) DTW and c) ESA. The warping paths between each signal pair for d) DTW and e) ESA alignment, respectively. The DTW distance and the phase (D_x) and amplitude (D_y) of ESA are indicated in the lower right corners. f) The CC before (squares) and after DTW (diamond) and ESA (cross) alignment.

Figure 2-2 illustrates the results obtained when applying DTW with Pearson CC distance (DTW-pcc) to the same waveforms. The DTW-pcc distances are smallest for the earthquake signal pair, consistent with the results from DTW and ESA. Additionally, we consider Pearson CC distances obtained from different correlation time windows ranging from 1 to 4 s, selected to be approximately shorter than the signal period. A larger correlation time window ($2L$) for the Pearson CC results in higher warping distances for all signal pairs. Moreover, the CCs of the signal pairs aligned by DTW-pcc are comparable to those obtained from ESA but lower than those from DTW. The CC values of the warped signal pairs increase with a larger correlation window. The DTW-pcc approach tends to yield higher CC values for the earthquake pair compared to ESA, but it does not increase CC for dissimilar source pairs as much as DTW, which is a desirable outcome.

To assist the discrimination of different underground source types, we introduce an additional distance metric known as the 'time distortion coefficient' (TDC). This novel metric is designed to

improve time series classification by measuring the type and degree of time distortion—such as compression, matching, and stretch alignments—between time series at each point [19]. TDC can be directly calculated from the previously determined DTW warping path and can be easily applied to other DTW variations. The optimal outcome is to obtain a very low TDC for similar event pairs and a very high TDC for different event types. Here, we test whether the time distortion information between signals can aid in evaluating the similarity of source types.

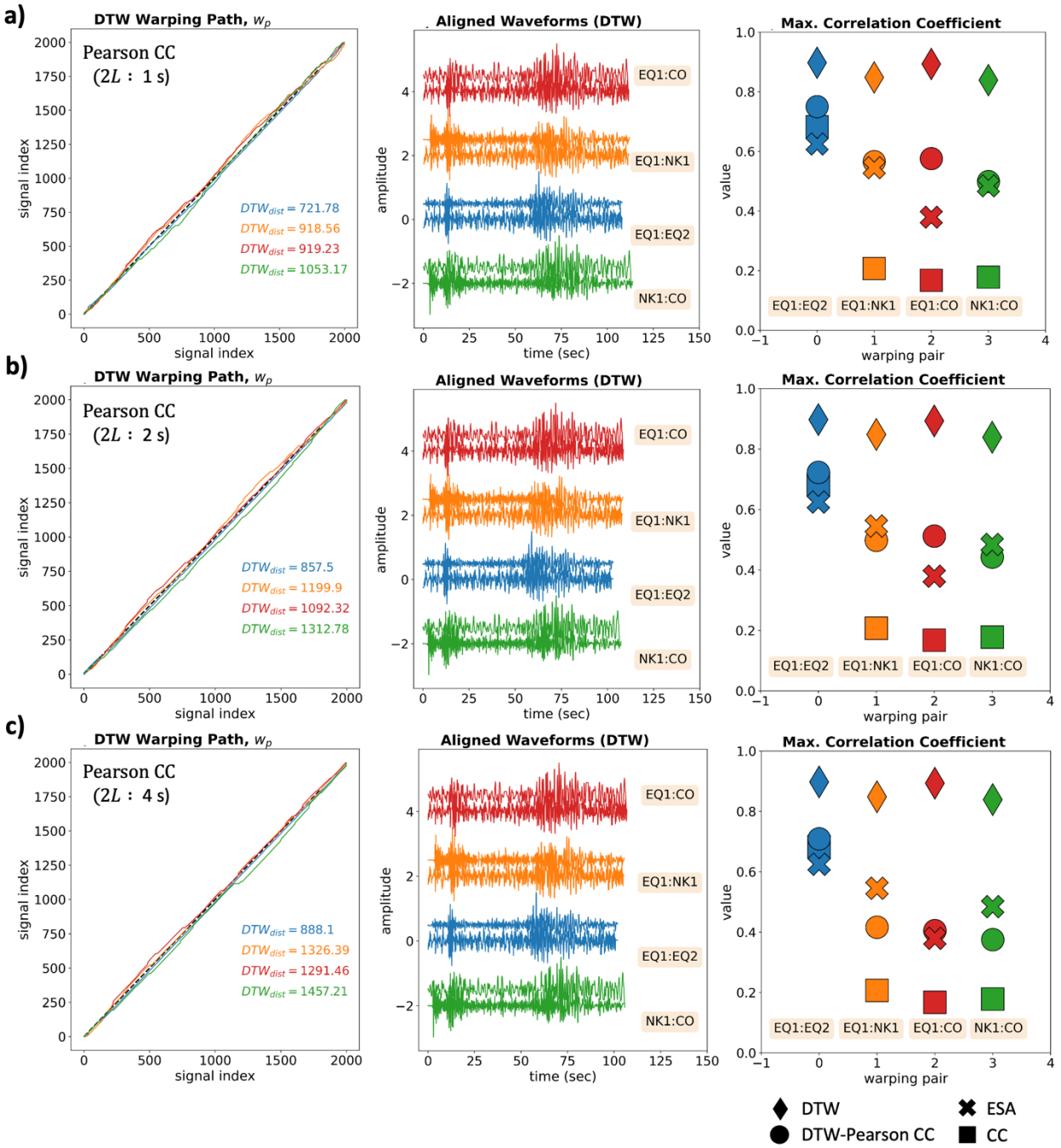

Figure 2-2. The warping paths and aligned waveforms, the CC (before (squares) and after alignments) between each signal pair by using DTW-pcc with a correlation time windows of a) 1 s, b) 2 s and c) 4 s. DTW distances are listed as inset.

Figure 2-3 shows the normalized warping distances and TDCs for the four waveform pairs. The TDCs are calculated using the warping paths from both DTW and DTW-pcc. While the TDC values closely resemble the DTW distances, they are significantly lower for the earthquake pair, as desired, when the DTW-pcc warping path is used ($2L = 2$ s, Figure 2-3c). This initial test encourages further investigations to determine whether TDC can serve as a robust additional metric in DTW-based source discrimination.

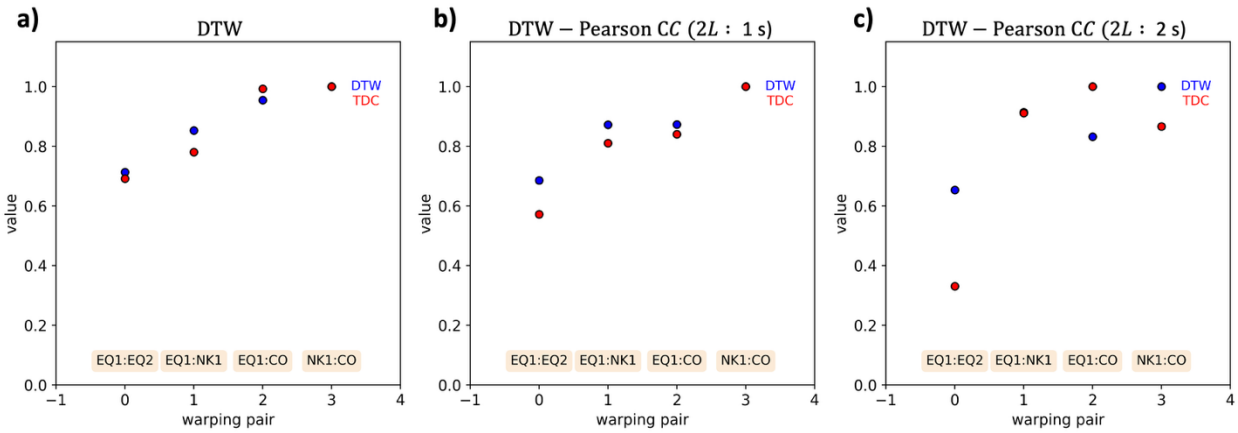

Figure 2-3. DTW and TDC distances for each event pair in Figure 2-1 obtained from a) traditional DTW, and DTW-pcc using correlation time windows of b) 1 s and c) 2 s.

We next consider a larger set of waveforms recorded at station MDJ, including 20 waveforms from earthquakes, explosions, and collapses (Figure 2-4). All events are located in the same small source region, which allows for the assumption that path effects are nearly identical from their hypocenters to station MDJ. The waveforms, filtered between 0.8 and 5 Hz, are used to obtain DTW and ESA distances between each signal pair. Note that the minor differences between our results and the reference study [14] are due to the fact that we use traditional DTW in our analysis rather than fastDTW. The matrix representation of the DTW distance and the ESA's amplitude distance (D_y) show smaller warping distances for the group of the explosion events (Figure 2-5a and c). This forms a strong structure in the matrix while it is less prominent for the earthquake pairs.

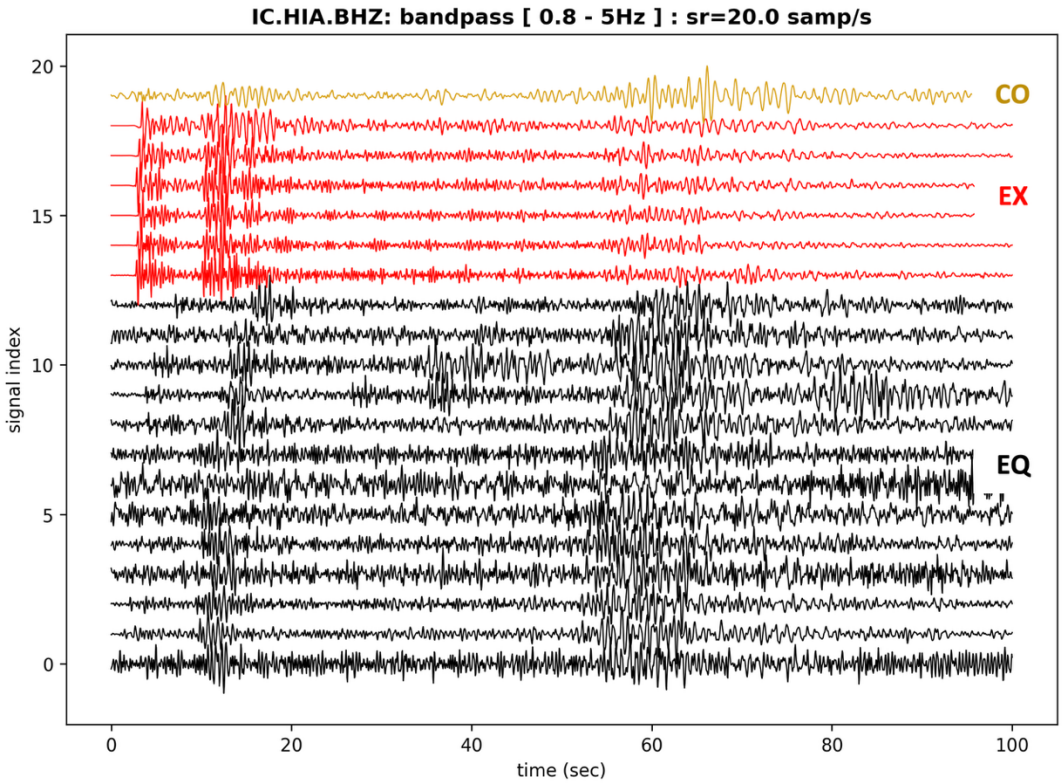

Figure 2-4. Vertical-component waveforms recorded at station MDJ filtered between 0.8 and 5 Hz, including earthquakes (0 – 12), explosions (13 – 18) and collapse (19). The explosions are the declared 2006 (NK1), 2009 (NK2), 2013 (NK3), 2016 (NK4, NK5), and 2017 (NK6) nuclear tests in the Korean Peninsula.

We also apply hierarchical clustering analysis to the DTW and ESA distances (Figure 2-5d and e). The common method for determining the optimal number of clusters in a dendrogram involves two main steps. First, identify the longest vertical line that does not intersect with any other cluster. Next, draw a horizontal line across the dendrogram at a chosen height, ideally half the length of this vertical line. The number of vertical lines intersected by this horizontal line can then be considered as the number of clusters. Both DTW and ESA suggest two clusters for the dataset. While DTW identifies the explosion events (13 – 18) as a separate cluster, ESA categorizes them as a sub-cluster within our analysis ($\tau =$ 0.8). Unfortunately, the dendrogram obtained from the DTW-pcc distances did not show robust clusters corresponding to the event source types for this dataset (Figure 2-5f). The DTW-pcc distance matrix reveals some structure only for parts of the explosion and earthquake groups.

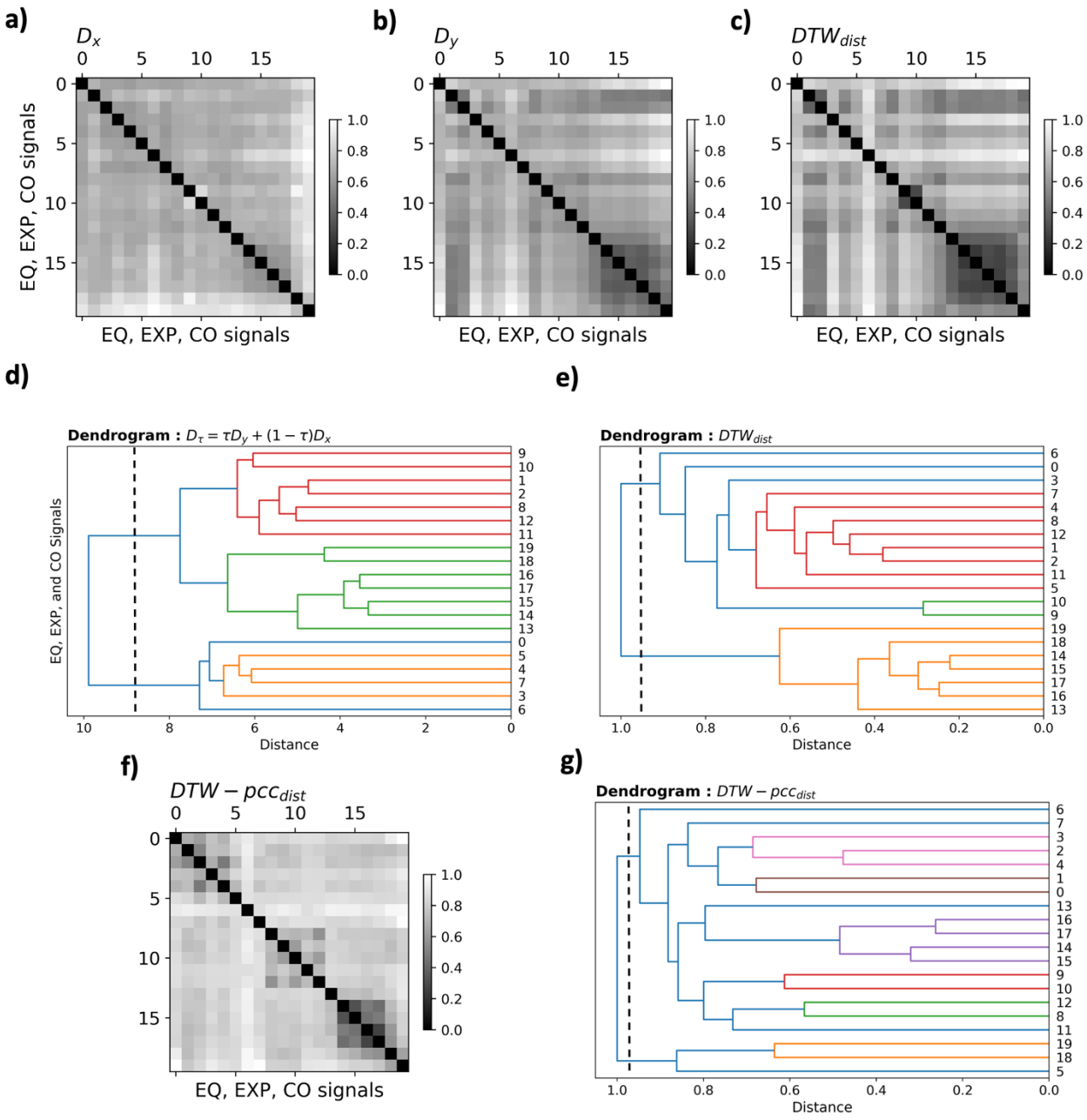

Figure 2-5. a) Phase (D_x) and b) amplitude (D_y) distance of ESA and c) DTW distance between every earthquake and explosion signal pair. Their corresponding dendrograms from hierarchical clustering analysis are shown in d) and e), respectively. f) Warping distances of each signal pair obtained using DTW-pcc ($2L = 2$ s) and g) its dendrogram. Threshold cutoffs are indicated as dashed lines on dendrograms, cutting through the half of the longest vertical line that does not intersect with any other cluster.

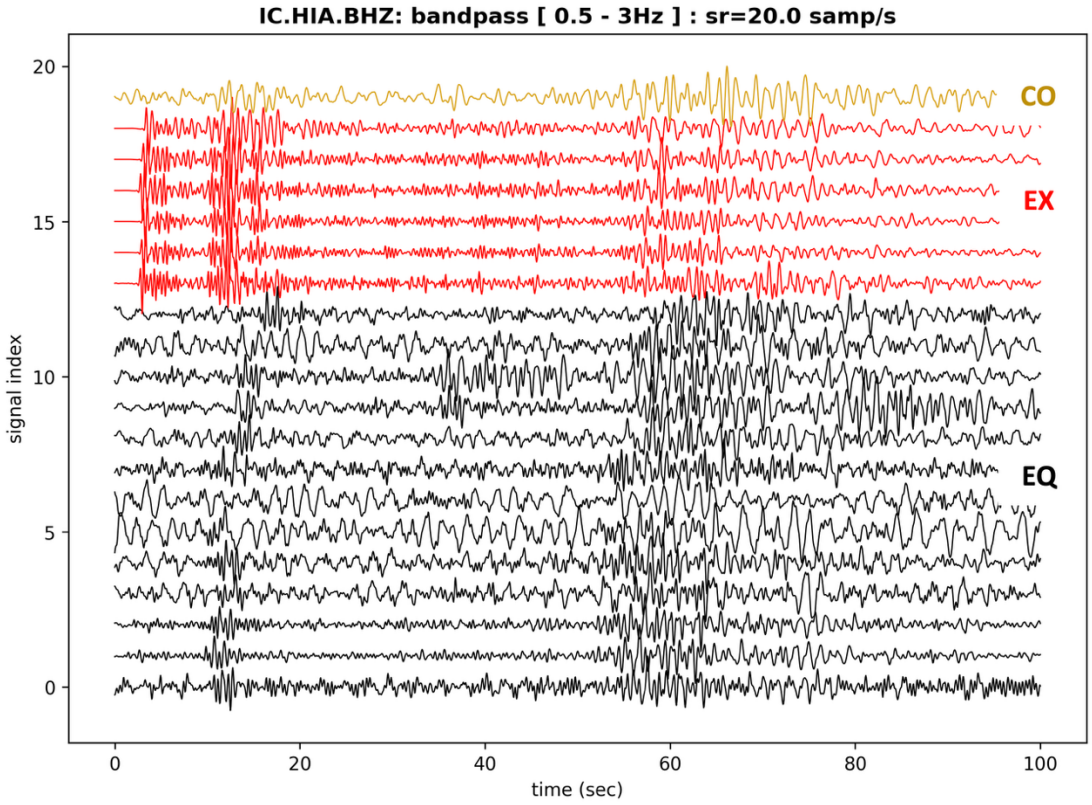

Figure 2-6. Vertical-component waveforms recorded at station MDJ (in Figure 2-4) filtered within a lower frequency band of 0.5 and 3 Hz.

To investigate whether the frequency band affects the performance of DTW-pcc, we applied a lower frequency range 0.5 to 3 Hz bandpass filter to the dataset at (Figure 2-6) and repeated the analysis. The matrix of DTW-pcc distances exhibited more prominent structures for both explosions and earthquakes at this frequency band. While this resulted in more defined clusters, the accuracy of the clustering analysis did not improve compared to the performance of DTW and ESA at the higher frequency band (Figure 2-7).

Furthermore, for the lower frequency band, the dendrograms for both DTW and ESA reveal significantly different clusters (Figure 2-7d and e) compared to those at the higher frequency band, suggesting that DTW and ESA are highly sensitive to the passbands of the waveforms. Therefore, careful selection of the filtering band is essential to achieve reasonable source classification performance. Additionally, we consider the matrix representations of TDC obtained from DTW and DTW-pcc in Figure 2-5. Figure 2-8 shows that both matrices indicate a structure with smaller TDC values corresponding to the group of explosion event pairs; however, TDC does not provide any additional or enhanced insight regarding the source type for this dataset.

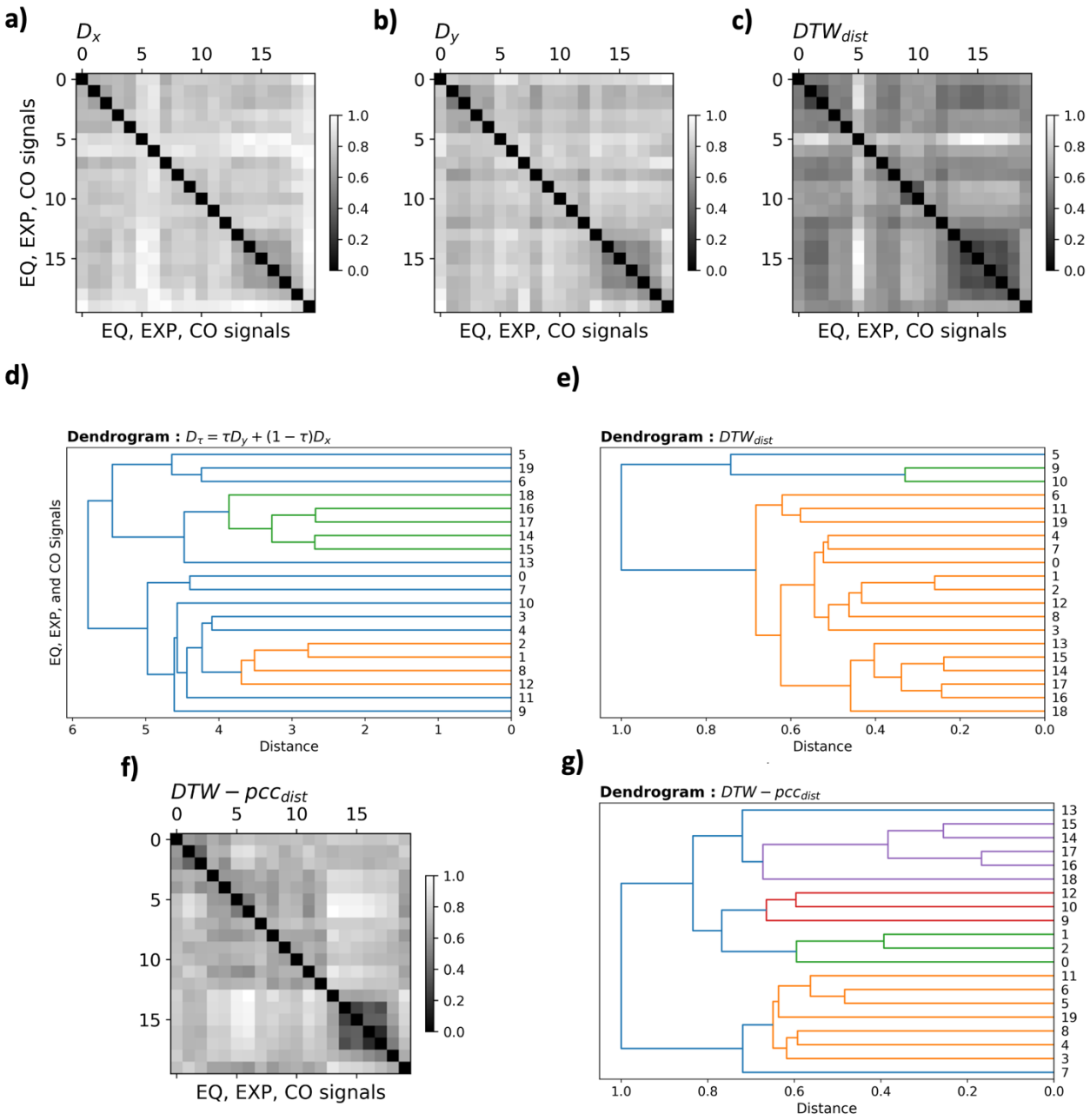

Figure 2-7. a) Phase (D_x) and b) amplitude (D_y) distance of ESA and c) DTW distance between every earthquake and explosion signal pair filtered with a lower frequency band (Figure 2-6). Their corresponding dendrograms from hierarchical clustering analysis are shown in d) and e), respectively. f) Warping distances of each signal pair obtained using DTW-pcc ($2L = 2$ s) and g) its dendrogram.

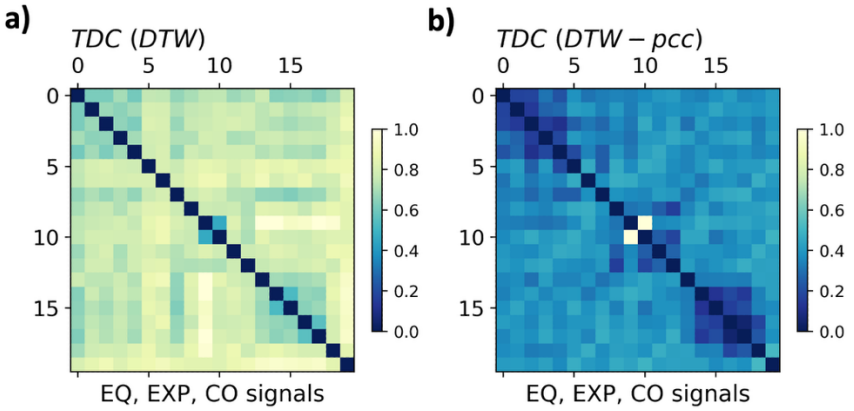

Figure 2-8. TDC distances between each signal pair in Figure 2-4 obtained using a) traditional DTW and b) DTW-pcc ($2L = 2$ s).

2.2. Clustering the cross-correlation of warped signals

We investigate using the CC of the warped waveforms instead of DTW and ESA distances in the cluster analysis to improve the source discrimination. Specifically, we evaluate whether the CC matrices exhibit more prominent structures that can aid in the cluster analysis of dendrograms. Using the same waveforms filtered between 0.8 and 5 Hz as in the previous section, we calculate the CC for each signal pair after warping. Here, we employ traditional DTW and ESA to warp and align the signals.

Figure 2-9 presents the CC matrices for the unwarped signal pairs in Figure 2-4, as well as for the signals aligned by ESA and DTW, respectively. While the initial CC matrix displays scattered structures, the CC matrices obtained after both DTW and ESA clearly reveal more robust structures that correspond to the three different groups of events. It is important to note that ESA does not yield a symmetric CC matrix, as the ESA distance varies depending on the reference waveform.

The dendrograms based on the CC after DTW and ESA indicate event clusters more distinctly than those obtained using DTW and ESA distances. Notably, the dendrogram from DTW successfully clusters all explosion and earthquake events into discrete groups, with the exception of a single collapse event. Our results demonstrate that employing the CC of the warped waveforms in dendrogram clustering (Figure 2-9b and c) outperforms clustering based on DTW and ESA distances (Figure 2-7d and e) used in the previous study for source discrimination in this regional seismic dataset.

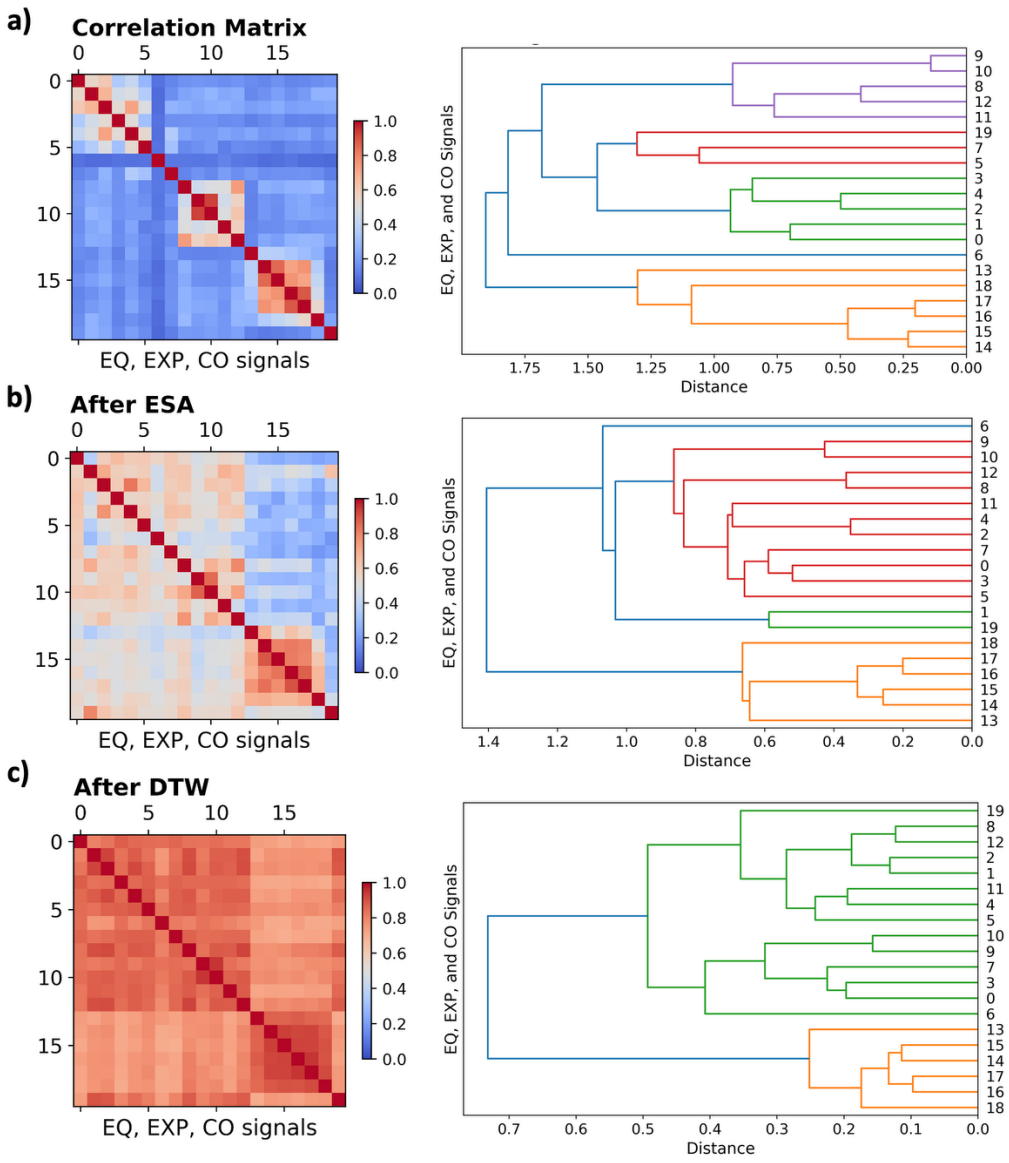

Figure 2-9. a) CC before alignment, b) after ESA and c) DTW alignments for each signal pair in Figure 2-4, along with their corresponding dendrograms from hierarchical clustering analysis.

3. EVALUATING DTW-BASED DISCRIMINATION AT LOCAL SCALES

To evaluate whether the waveform warping discrimination results from the Korean Peninsula transfer to other regions and other source-receiver distances, we analyze a subset of the Utah Unconstrained Event Bulletin (UUEB) dataset [20]. This high-quality catalog spans a two-week period and includes both tectonic and anthropogenic events, making it particularly useful for testing event discrimination methods. By focusing on the events with more confidently labeled source types, we concentrate on one earthquake cluster and one explosion-like cluster (quarry blasts) located within a 1-degree radius area (Figure 3-1). The clusters comprise a total of 46 events, including 17 earthquake and 29 explosion-like sources.

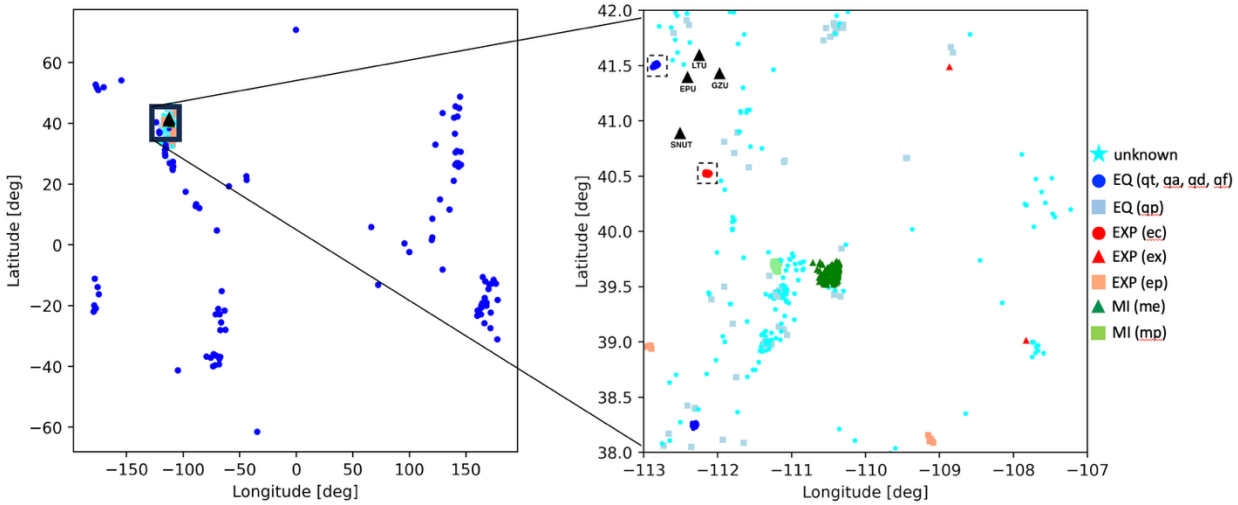

Figure 3-1. UUEB catalog events. The map (right) provides a closer view of the events. Clusters highlighted by dashed squares are included in the analysis. Black triangles indicate some of the nearby stations.

We utilize waveforms from station SNUT (Network UU) to assess the performance of using CCs after warping in cluster analysis for event type discrimination. Due to the distance between the two clusters, there may be potential path effects in addition to source type effects. This station recorded high signal-to-noise ratio signals for the events (Figure 3-2a). The vertical-component waveforms are bandpass filtered between 2 and 10 Hz, and we consider 25-s time windows following the origin time of the events for DTW and ESA analysis. The distance matrices of ESA and DTW reveal a structure characterized by smaller warping distances corresponding to the group of earthquake event pairs (Figure 3-2b and d).

Next, we calculate the CC for each signal pair using the unwarped signals and the warped signals (Figure 3-3). While all CC matrices reveal a high-correlation structure for the earthquake group, the explosion event group is more distinctly defined in the CC matrices obtained after ESA and DTW. Nonetheless, the accuracy of event type clustering across all dendrograms is very good, and in fact the version based on correlation of the unwarped waveforms seems to produce the best separation of the two groups, suggesting that the use of DTW or ESA may not actually improve discrimination capability for this set of local-distance events.

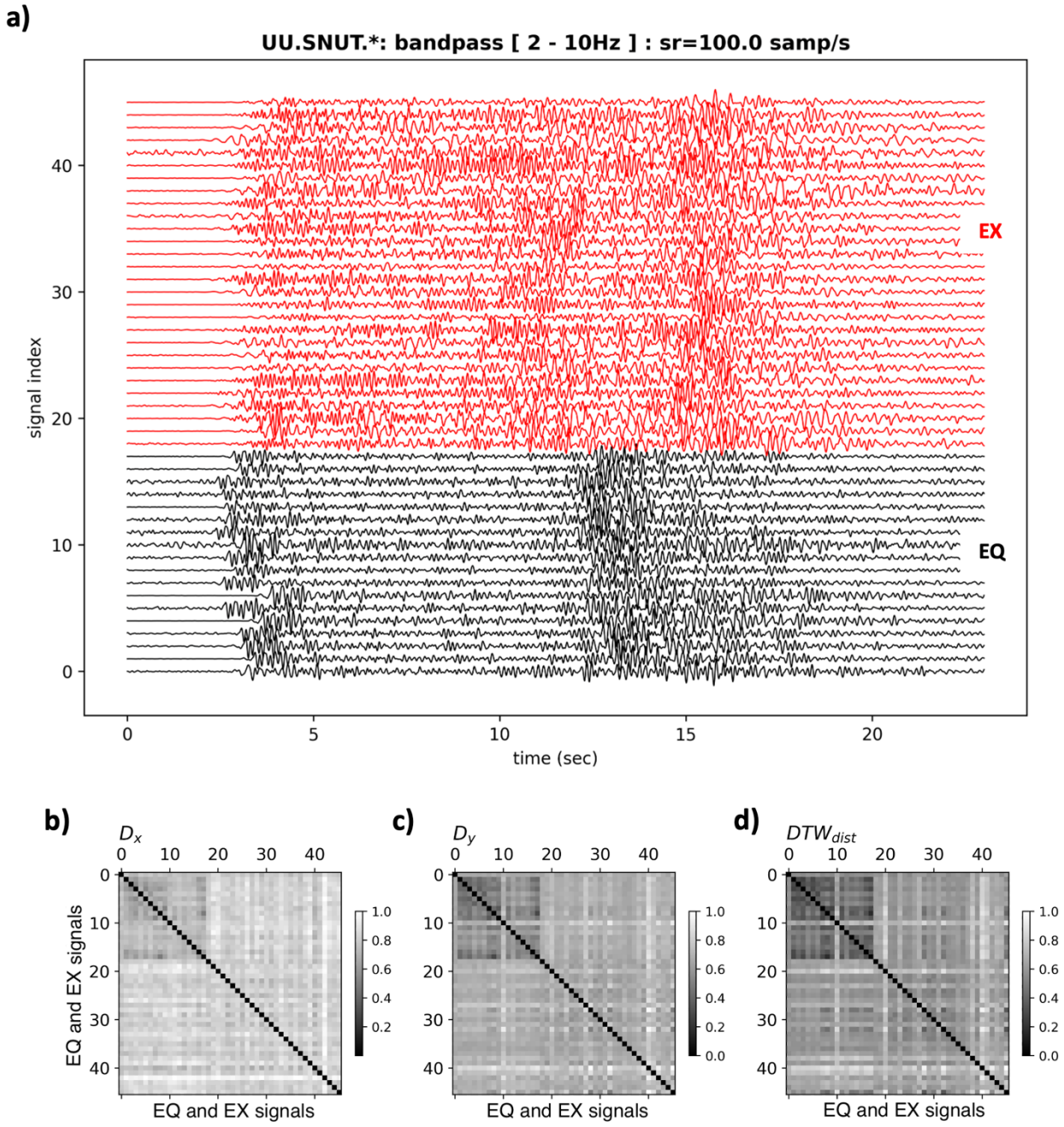

Figure 3-2. a) Vertical-component waveforms recorded at station SNUT filtered between 2 and 10 Hz. b) Phase (D_x) and c) amplitude (D_y) distance of ESA and d) DTW distance between every earthquake and explosion-like event pairs.

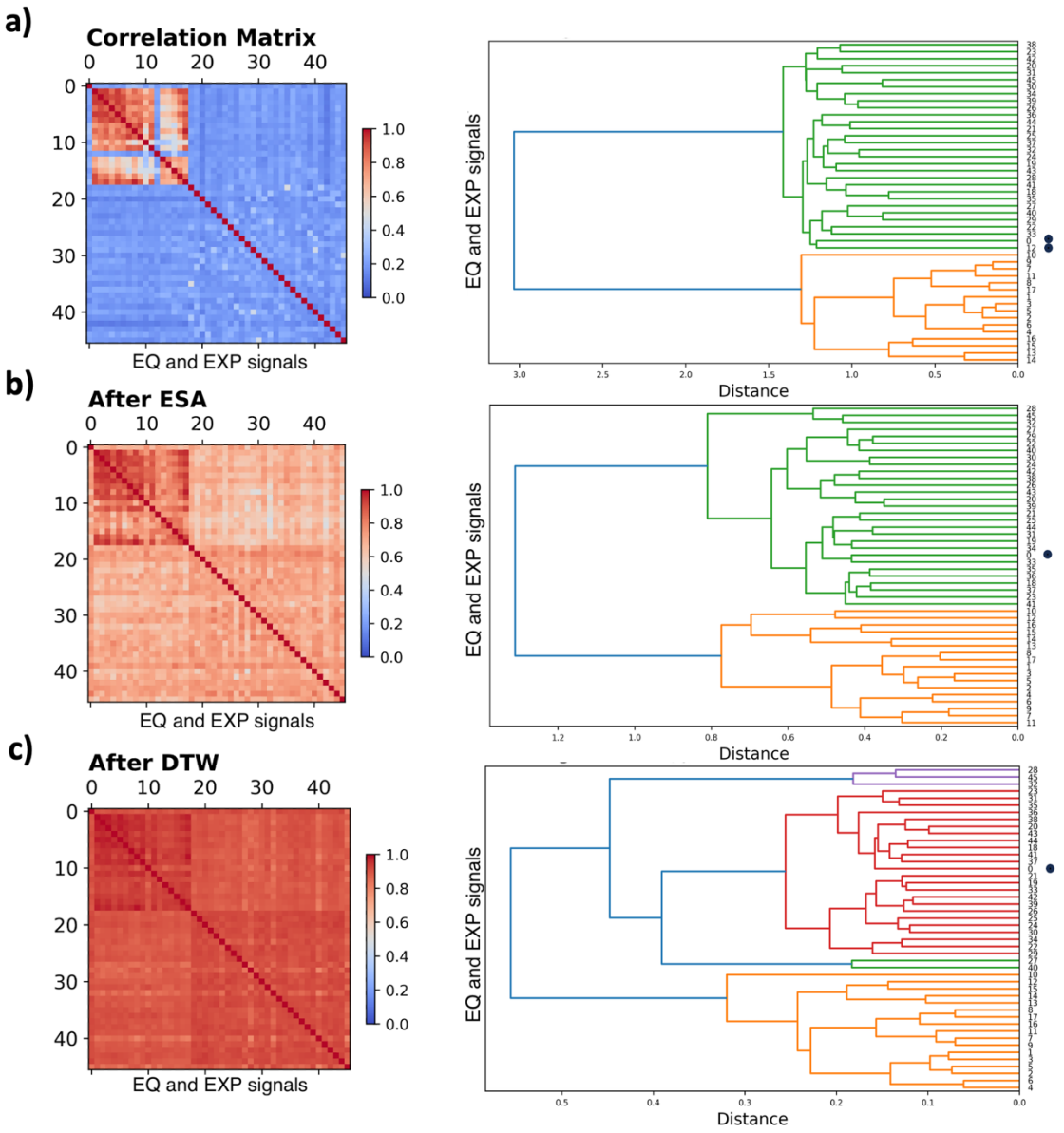

Figure 3-3. a) CC before alignment, b) after ESA and c) DTW alignments for each signal pair in Figure 3-2, along with their corresponding dendrograms from hierarchical clustering analysis. The black dots indicate the events that were misclassified in the dendrogram.

Additionally, we consider a dataset for cluster analysis that includes more significant amplitude changes due to source radiation patterns as well as noise spikes within the coda. The waveforms recorded at station EPU (UU) are filtered between 2 and 10 Hz (Figure 3-4a). The signal-to-noise ratios of the waveforms are relatively high, except for those with the noise spikes. The matrices of ESA and DTW distances reveal a smaller-distance structure for the earthquake group (Figure 3-4b and d). Furthermore, the matrices display large-distance bands corresponding to waveforms that are dissimilar to the rest of the events (e.g., signals 12, 18, and 41). The DTW distance and the

amplitude distance (D_y) from ESA produce very similar patterns on the matrices (Figure 3-4c and d).

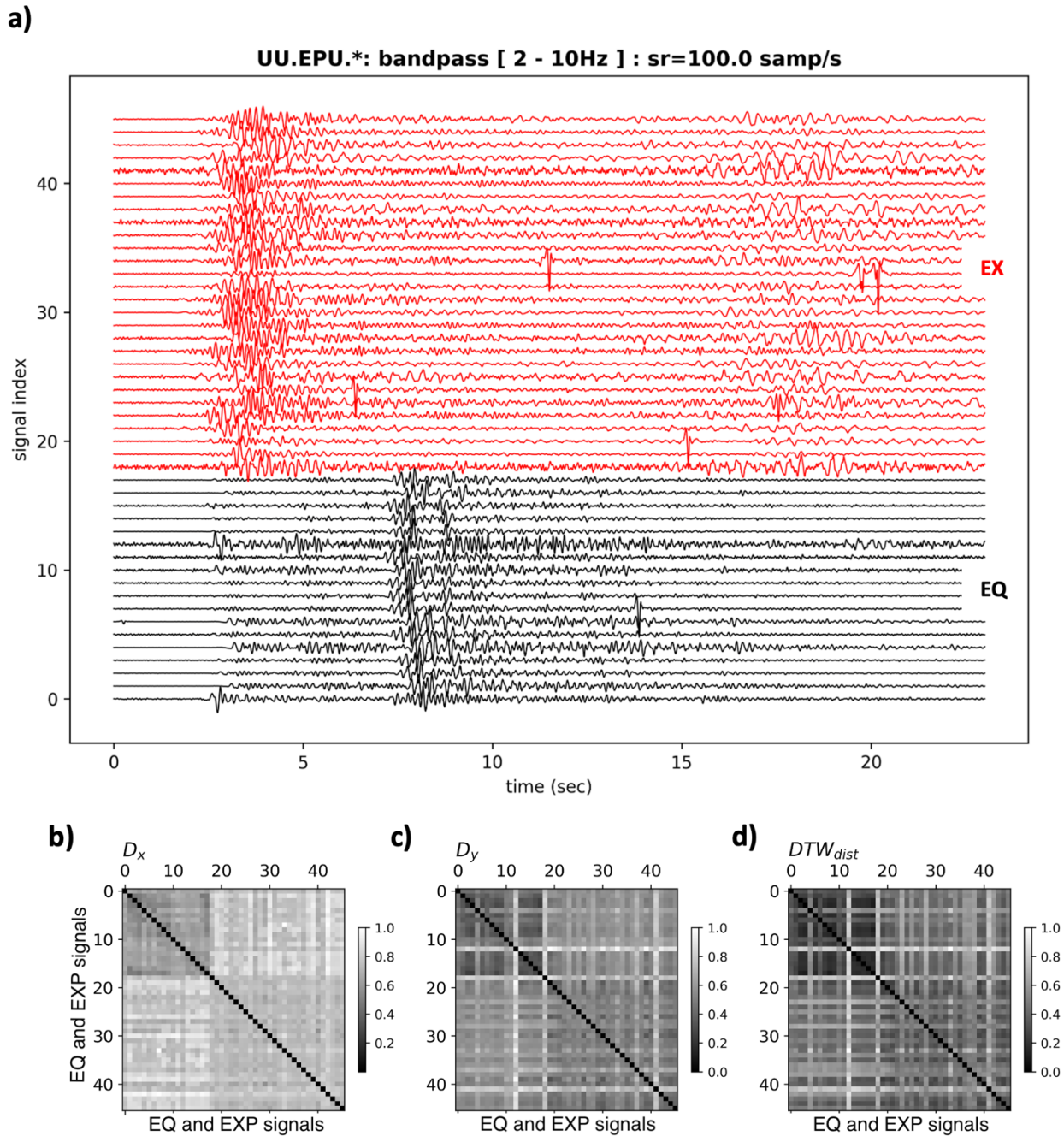

Figure 3-4. Vertical-component waveforms recorded at station EPU filtered between 2 and 10 Hz. b) Phase (D_x) and c) amplitude (D_y) distance of ESA and d) DTW distance between every earthquake and explosion-like event pairs.

The dendrogram clustering of CC matrices obtained using the warped and unwarped signals indicate that both the original signals and the signals aligned by ESA yield satisfactory clustering accuracy for the two source types, with only a few misclassified events (Figure 3-5). In contrast, the DTW-based clustering does not perform well for this dataset. To attempt to improve performance, we exclude the waveforms with noise spikes and shorten the time window to 14 seconds to eliminate sections of noisy data before repeating the clustering analysis (Figure 3-6). However, DTW-based clustering still cannot distinguish between different event types. This suggests that DTW-based clustering analysis is highly sensitive to low signal-to-noise ratios, source radiation patterns, and noise spikes, and may not perform satisfactorily for event type discrimination at local distances.

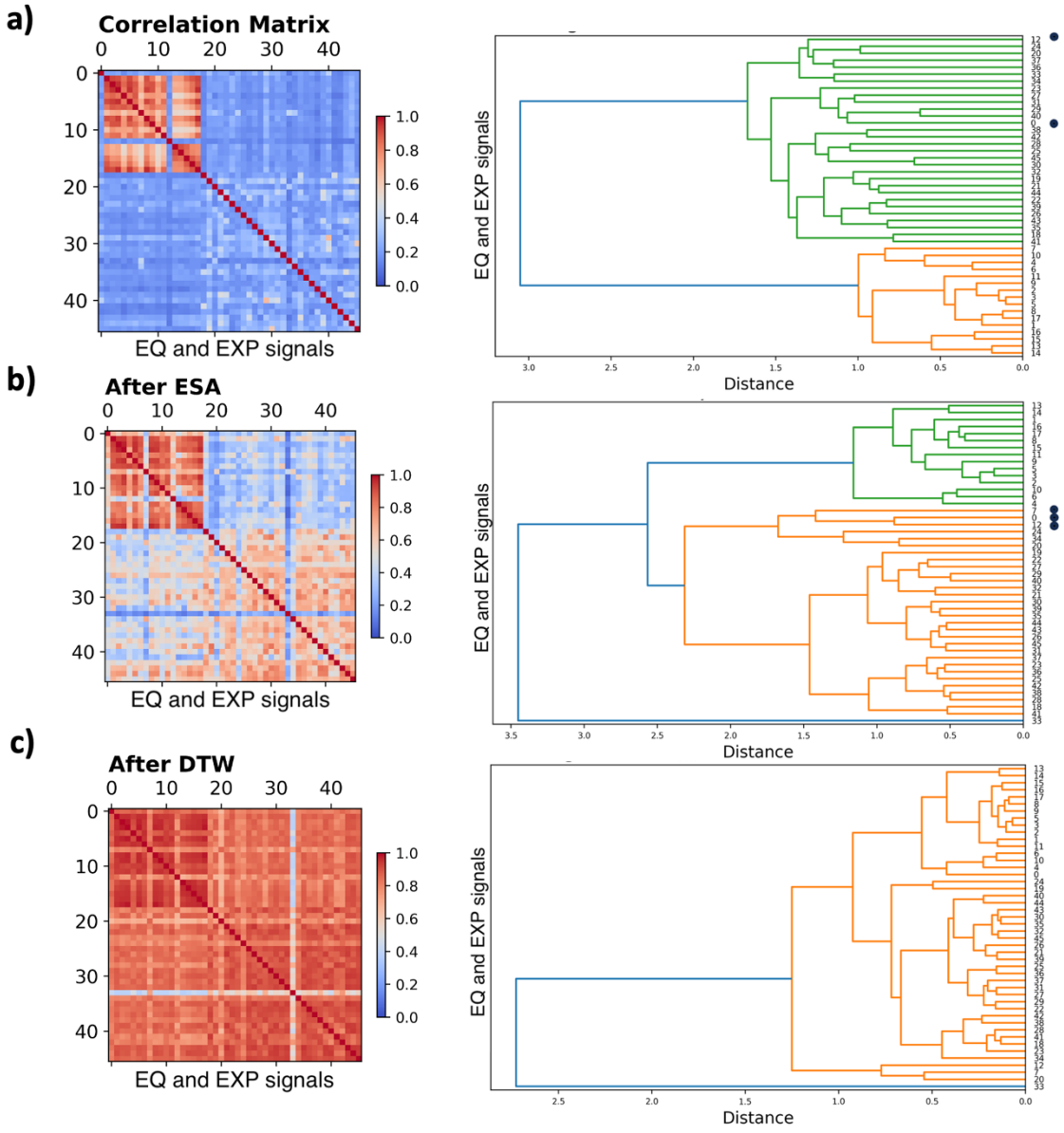

Figure 3-5. a) CC before alignment, b) after ESA and c) DTW alignments for each signal pair in Figure 3-4, along with their corresponding dendrograms from hierarchical clustering analysis. The black dots indicate the events that were misclassified in the dendrogram (not shown for DTW).

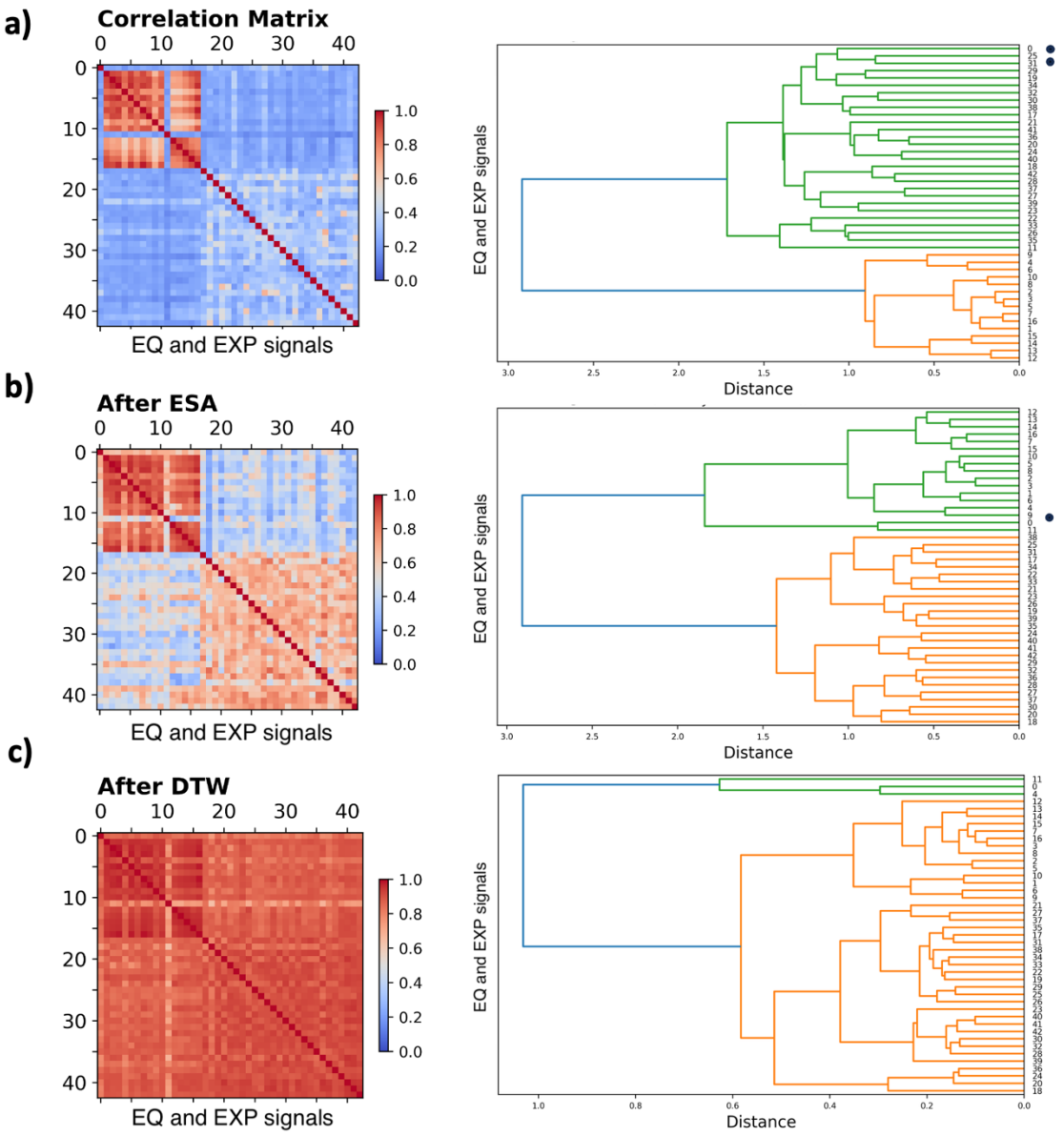

Figure 3-6. Following the exclusion of waveforms with noise spikes, a) CC before alignment, b) after ESA and c) DTW alignments for each signal pair in Figure 3-4, along with their corresponding dendrograms from hierarchical clustering analysis. The black dots indicate the events that were misclassified in the dendrogram (not shown for DTW).

Lastly, we investigate whether the warped signals consistently result in higher CC values. Our tests on the UUEB events indicate that the increase in signal similarity is not linearly proportional to the similarity of the original signals; in other words, a signal pair with a moderate CC can achieve the highest similarity in the group after warping. We present a single pair of earthquakes after alignment using ESA and DTW (Figure 3-7a). We observe that ESA dramatically modifies the waveform EQ4,

introducing a long-period swing prior to the first arrival in an attempt to better align with the EQ5 waveform. While DTW increases the similarity of the signals from 0.88 to 0.95, ESA actually decreases the similarity to 0.61 (Figure 3-7b), a troubling result for this high SNR pair of local-distance signals.

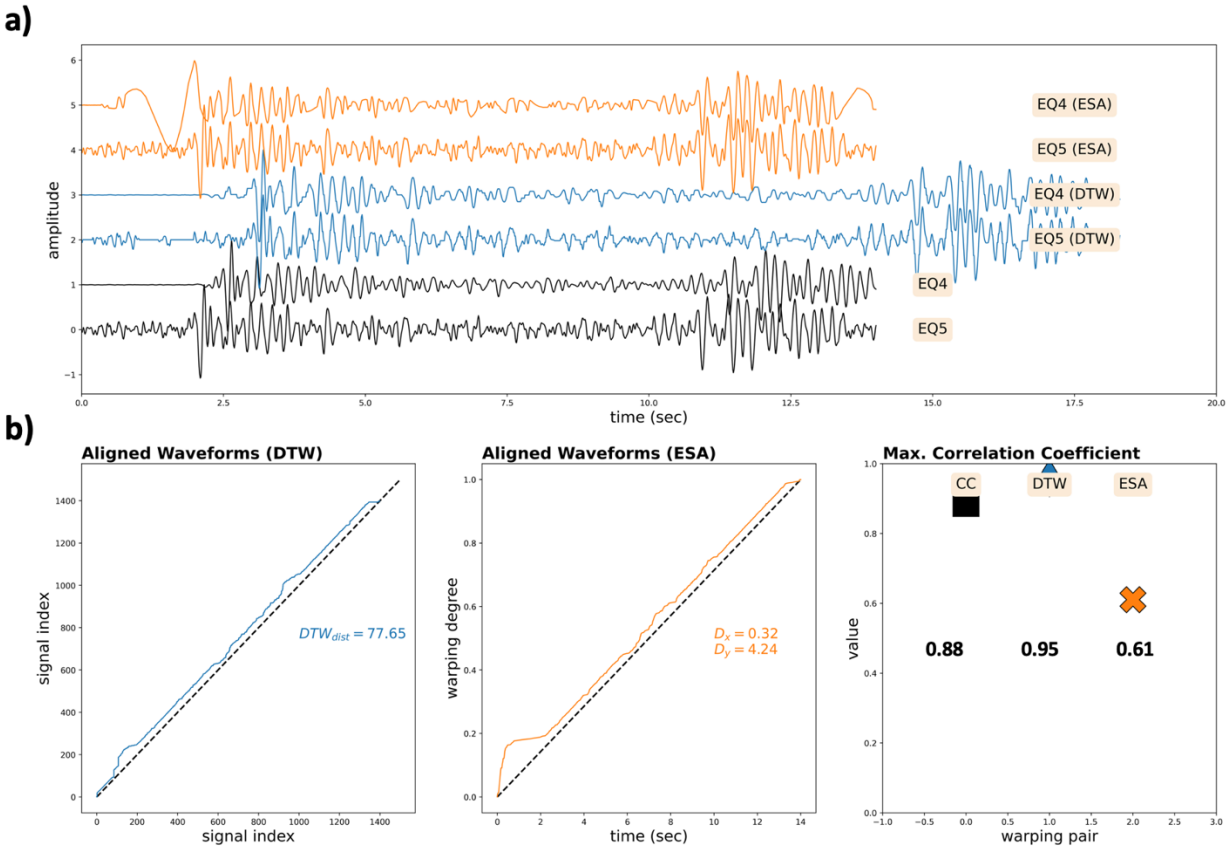

Figure 3-7. a) A pair of earthquake waveforms recorded at station GZU, displayed without any warping, alongside the aligned pairs obtained using DTW and ESA. b) The warping paths of DTW and ESA between the signal pair and the CC before (squares) and after DTW (diamond) and ESA (cross) alignment.

4. CONCLUSIONS

This study investigated the effectiveness of DTW and ESA as nonlinear alignment techniques for discriminating between different seismic event types from datasets in two different regions, one consisting of signals from regional source-receiver distances and the other consisting of signals from local distances. We evaluated the performance of two advanced DTW methods: one utilizing Pearson cross-correlation as a warping distance and the other employing a time distortion coefficient. Our analysis of the regional dataset from the Korean Peninsula, which included hierarchical cluster analysis and dendrogram interpretation, revealed that while the advanced DTW methods did not directly significantly enhance source discrimination, performing cluster analysis based on CCs of the warped waveforms did improve event classification accuracy. Notably, this enhancement was primarily observed at regional distances. In contrast, for our local distance dataset from Utah, the cross-correlation performance of warped waveforms did not produce any clear improvement over the cross-correlation of the original waveforms. Furthermore, we found that DTW-based clustering analysis is particularly sensitive to low signal-to-noise ratios, variations in source radiation patterns, and noise spikes, which may hinder its effectiveness in discriminating event types at local distances.

Our results suggest the importance of selecting appropriate warping techniques based on the observational distance. Future research should focus on refining these methods and exploring their applicability across diverse seismic environments to improve event discrimination capabilities.

REFERENCES

[1] C. Alvizuri and C. Tape, "Full moment tensor analysis of nuclear explosions in North Korea," *Seismological Research Letters,* vol. 89, no. 6, pp. 2139-2151, 2018.

[2] M. E. Pasyanos and A. Chiang, "Full moment tensor solutions of US underground nuclear tests for event screening and yield estimation," *Bulletin of the Seismological Society of America,* vol. 112, no. 1, pp. 538-552, 2022.

[3] J. L. Stevens and S. M. Day, "The physical basis of mb: Ms and variable frequency magnitude methods for earthquake/explosion discrimination," *Journal of Geophysical Research: Solid Earth,* vol. 90, no. B4, pp. 3009-3020, 1985.

[4] C. T. O'Rourke, G. E. Baker and A. F. Sheehan, "Using P/S amplitude ratios for seismic discrimination at local distances," *Bulletin of the Seismological Society of America,* vol. 106, no. 5, pp. 2320-2331, 2016.

[5] M. L. Pyle and W. R. Walter, "Investigating the effectiveness of P/S amplitude ratios for local distance event discrimination," *Bulletin of the Seismological Society of America ,* vol. 109, no. 3, pp. 1071-1081, 2019.

[6] R. Tibi, K. D. Koper, K. L. Pankow and C. J. Young, "Discrimination of anthropogenic events and tectonic earthquakes in Utah using a quadratic discriminant function approach with local distance amplitude ratios," *Bulletin of the Seismological Society of America,* vol. 108, no. 5A, pp. 2788-2800, 2018.

[7] R. Wang, B. Schmandt, M. Holt and K. Koper, "Advancing local distance discrimination of explosions and earthquakes with joint P/S and ML-MC classification," *Geophysical Research Letters,* vol. 48, no. 23, p. e2021GL095721, 2021.

[8] G. Eggertsson, B. Lund, M. Roth and P. Schmidt, "Earthquake or blast? Classification of local-distance seismic events in Sweden using fully connected neural networks," *Geophysical Journal International,* vol. 236, no. 3, pp. 1728-1742, 2024.

[9] L. Linville, K. Pankow and T. Draelos, "Deep learning models augment analyst decisions for event discrimination," *Geophysical Research Letters,* vol. 46, no. 7, pp. 3643-3651, 2019.

[10] R. Maguire, B. Schmandt, R. Wang, Q. Kong and P. Sanchez, "Generalization of deep-learning models for classification of local distance earthquakes and explosions across various geologic settings," *Seismological Research Letters,* vol. 95, no. 4, pp. 2229-2238, 2024.

[11] S. Rathnayaka, A. Nyblade, B. Lund, C. Ammon, R. Durrheim and R. Maseth, "Testing the P/S amplitude seismic source discriminant at local distances using seismic events within and surrounding the Kloof Gold Mine, South Africa, and the Kiruna Iron Ore Mine, Northern Sweden," *Bulletin of the Seismological Society of America,* vol. 114, no. 4, pp. 2237-2250, 2024.

[12] S. Rathnayaka, R. Maguire, A. Nyblade, B. Lund and B. Schmandt, "Convolutional Neural Networks Versus P/S Amplitude Ratios in Low-Yield Seismic Event Discrimination: An Evaluation Using Earthquakes, Mine Blasts, and Mining-Related Events from the Kiruna Mining Region, Northern Sweden," *Seismological Research Letters,* 2025.

[13] R. Tibi, N. Downey and R. Brogan, "Testing and design of discriminants for local seismic events recorded during the Redmond salt mine monitoring experiment," *Bulletin of the Seismological Society of America,* vol. 114, no. 2, pp. 906-923, 2024.

[14] M. D. Ramos, R. Tibi, C. J. Young and E. L. Emry, "Regional Source-Type Discrimination Using Nonlinear Alignment Algorithms," *The Seismic Record,* vol. 5, no. 1, pp. 97-106, 2025.

[15] S. Salvador and P. Chan, "Toward accurate dynamic time warping in linear time and space," *Intelligent data analysis,* vol. 11, no. 5, pp. 561-580, 2007.

[16] M. Müller, Information retrieval for music and motion, Berlin: Springer Berlin Heidelberg, 2007.

[17] J. Zhao and L. Itti, "shapeDTW: Shape dynamic time warping," *Pattern Recognition,* vol. 74, pp. 171-184, 2018.

[18] X. Guo, Y. Yu and M. Sun, "Improving earthquake location resolution through dynamic time warping-based crosscorrelation," *Geophysics,* vol. 90, no. 3, pp. L85-L98, 2025.

[19] Y. Liu, Y.-A. Zhang, M. Zeng and J. Zhao, "A novel distance measure based on dynamic time warping to improve time series classification," *Information Sciences,* vol. 656, p. 119921, 2024.

[20] L. Linville, R. C. Brogan, C. Young and K. A. Aur, "Global-and local-scale high-resolution event catalogs for algorithm testing," *Seismological Research Letters,* vol. 90, no. 5, pp. 1987-1993, 2019.

[21] H. Sakoe and S. Chiba, "Dynamic programming algorithm optimization for spoken word recognition," *IEEE transactions on acoustics, speech, and signal processing,* vol. 26, no. 1, pp. 43-49, 2003.

[22] M. Müller, Fundamentals of music processing: Using Python and Jupyter notebooks, Springer, 2021.

[23] J. D. Tucker, W. Wu and A. Srivastava, "Generative models for functional data using phase and amplitude separation," *Computational Statistics & Data Analysis,* vol. 61, pp. 50-66, 2013.

[24] R. Tibi, "Discrimination of seismic events (2006–2020) in North Korea using P/Lg amplitude ratios from regional stations and a bivariate discriminant function," *Seismological Society of America,* vol. 92, no. 4, pp. 2399-2409, 2021.

DISTRIBUTION

Email—Internal

Name	Org.	Sandia Email Address
G. Didem Beskardes	8911	gdbeska@sandia.gov
Rigobert Tibi	6756	rtibi@sandia.gov
Christopher J. Young	N/A	cjyoung@sandia.gov
Erica L. Emry	6752	elemry@sandia.gov
Technical Library	1911	sanddocs@sandia.gov

This page left blank

Sandia National Laboratories

Sandia National Laboratories is a multimission laboratory managed and operated by National Technology & Engineering Solutions of Sandia LLC, a wholly owned subsidiary of Honeywell International Inc. for the U.S. Department of Energy's National Nuclear Security Administration under contract DE-NA0003525.